Enhanced Electro-optic Sampling with Quantum Probes

Stéphane Virally,* Patrick Cusson, and Denis V. Seletskiy†
femtoQ Lab, Engineering Physics Department, Polytechnique Montréal, Montréal, Québec H3T 1JK, Canada

(Received 15 June 2021; accepted 9 December 2021; published 30 December 2021)

Employing electro-optic sampling (EOS) with ultrashort probe pulses, recent experiments showed direct measurements of quantum vacuum fields and their correlations on subcycle timescales. Here, we propose a quantum-enhanced EOS where bright photon-number entangled twin beams are used to derive conditioned nonclassical probes. In the case of the quantum vacuum, this leads to a sixfold improvement in the signal-to-noise ratio over the classically probed EOS. In addition, engineering of the conditioning protocol yields a reliable way to extract higher-order moments of the quantum noise distribution and robust discrimination of the input quantum states, for instance, a vacuum and a few-photon cat state. These improvements open a viable route toward robust tomography of quantum fields in space-time, an equivalent of homodyne detection in energy-momentum space, and the possibility of precise experiments in real-space quantum electrodynamics.

DOI: 10.1103/PhysRevLett.127.270504

The underlying relativistic invariance of quantum electrodynamics is best manifested when nonclassical fields are expressed directly in space-time coordinates [1]. Yet, most measurement methods of quantum fields are intrinsically rooted in the reciprocal (energy-momentum) space, following a first quantization step with the Hamiltonian method. Such is the case of homodyne detection (HD) [2] in quantum optics, where information on the quantum state is obtained by registering in a square-law detector its linear superposition with a narrow band classical field, also termed "local oscillator" (LO). In these measurements, nonvanishing signals only arise where both inputs are commensurate in angular frequency and wave vector ($\Delta\omega \simeq 0$, $\Delta k \simeq 0$).

For direct space-time measurement of electromagnetic fields, it is necessary to (1) replace the narrow band LO by a short, wideband probe and (2) augment the optical superposition of HD by a wave mixing of the probe and signal. In addition, for quantum signals, one needs to access all moments of the statistics of the measured field amplitude, in the same way that HD with a sufficiently strong LO enables full tomography of quantum states in the frequency domain [3].

The first two requirements are fulfilled in a scenario where a low-frequency signal (Ω, e.g., in the THz range) is nonlinearly mixed with a short probe of duration Δt at a higher carrier frequency [ω, e.g., in the near-infrared (NIR) region]. The subcycle structure of the THz field can be probed when $\Omega\Delta t < 1/2$ and both fields are overlapped within a small space-time volume ($\Delta t \simeq 0$, $\Delta r \simeq 0$) [4]. This setup is at the heart of the electro-optic sampling (EOS) scheme, where the measurement of the instantaneous electric amplitude $\mathcal{E}_{\mathrm{THz}}(t)$ of a classical field is made possible by superposing the weak nonlinear mixing product between this field and the probe, with the strong noninteracted part of the probe [5]. Thanks to advances in femtosecond laser technologies [6–8], shortening of the probe duration has enabled progress of EOS from sub-terahertz (THz) frequencies [9] to detection of fields with Ω components extending to 100 THz and above [10–17], in turn empowering field-resolved spectroscopies [18,19].

In contrast to HD, it is very difficult to measure a weak signal such as a quantum state $|\psi_{\mathrm{THz}}\rangle$ with EOS. In HD, a strong LO can amplify the signal, but in EOS the nonlinear mixing products must remain intrinsically weak to avoid noise induced by higher-order processes. Nonetheless, recent experiments have ported EOS with classical probes to the quantum regime, measuring the variance $\langle\psi|\hat{\mathcal{E}}^2(t)|\psi\rangle$ [4,20] and two-time correlations $\langle\psi|\hat{\mathcal{E}}(t_1)\hat{\mathcal{E}}(t_2)|\psi\rangle$ [21,22] of broadband THz vacuum fields. Such measurements are limited by the shot noise of the probe [23], and the contribution of the quantum signal $|\psi\rangle$ amounts only to a few percent of the total detected noise [4,24]. This impedes the determination of high statistical moments of the quantum distribution, which is further exacerbated by the Gaussian statistics of the classical probe pulses.

In this Letter, we show that EOS of quantum fields can be dramatically improved by employing quantum probe pulses. Specifically, entangled bright few-cycle pulses [25,26] originating from parametric down-conversion (PDC) can be used to carve out nonclassical statistics [27] in a probe beam by conditioning it on intensity values of its twin. Because the conditioning only selects events in certain bands of intensities, we refer to these nonclassical states as band-conditioned states (BCSs). Compared to classical EOS probes, BCSs not only provide a sixfold improvement in the detection of the variance, but also extract additional information on higher statistical moments

of the quantum distribution by simple modifications of the conditioning protocol. This enables robust sampling of non-Gaussian subcycle states of quantum light, for instance, a few-photon cat state. Thanks to these features, BCSs are well positioned to fulfill the needs of characterization of time-domain quantum optical beams [28] and emerging applications in time-domain quantum spectroscopy [29–32].

In order to compare classical and quantum-enhanced detection, we start with the operational principle of EOS using coherent state $|\alpha\rangle$ probes. As sketched in Fig. 1(a), a train of NIR probe pulses ($\ldots, i, i+1, \ldots$, in blue) is mixed with a train of identically prepared THz quantum states $|\Psi_{\mathrm{THz}}\rangle$ (in red) through second-order nonlinear interaction inside an electro-optic crystal (EOX). THz-induced birefringence changes the polarization state of the pulsed probe, which is directly proportional to either the amplitude or the Hilbert transform of the THz electric field signal [28,33]. For the amplitude measurement, polarization change is converted by an ellipsometer [a quarter wave plate (QWP) followed by a polarizing beam splitter (PBS)] into an imbalance of photocounts Δn_i and registered by a balanced photodiode (BPD) pair [5]. The temporal delay τ introduced between the probe and the signal pulses allows for sampling of field statistics at controlled time slices. In terms of the probe's polarization state, the effect of EOS (EOX, QWP, PBS) can be mapped onto an effective "nonlinear beam splitter" (NLBS), where the THz amplitude induces an imbalance in an otherwise equal splitting of the probe [Fig. 1(a)]. Specifically, the EOS signal is directly proportional to the photocount difference between the two output ports of the NLBS, where the splitting ratio after the ellipsometer is dictated by the amplitude of the THz field in accordance with the linearized $\chi^{(2)}$ model [5,23]. For small THz input, this signal is directly proportional to the THz amplitude (see Supplemental Material [34]).

For an incident signal ψ, the BPD pair after the NLBS registers Δn with a probability $P(\Delta n;\psi)$, which takes the form

$$P(\Delta n;\psi) = \sum_{n=0}^{+\infty} P(n) \sum_{k=0}^{+\infty} a_k(n,\Delta n)\langle\psi|\hat{\mathcal{E}}^k|\psi\rangle, \quad (1)$$

where $P(n)$ is the probability of having n photons in the probe, $\langle\psi|\hat{\mathcal{E}}^k|\psi\rangle$ is the kth moment of the electric field distribution in the signal, and the a_k are coefficients dependent on the particulars of the setup [34]. Equation (1) highlights two main contributions to $P(\Delta n;\psi)$: (i) the second-quantization photocount distribution of the probe and (ii) the statistical distribution of the THz electric field, as a parameter in the binomial distribution characteristic of the NLBS. Isolation of the contribution of the quantum signal can be made by decoupling it from the probe through a

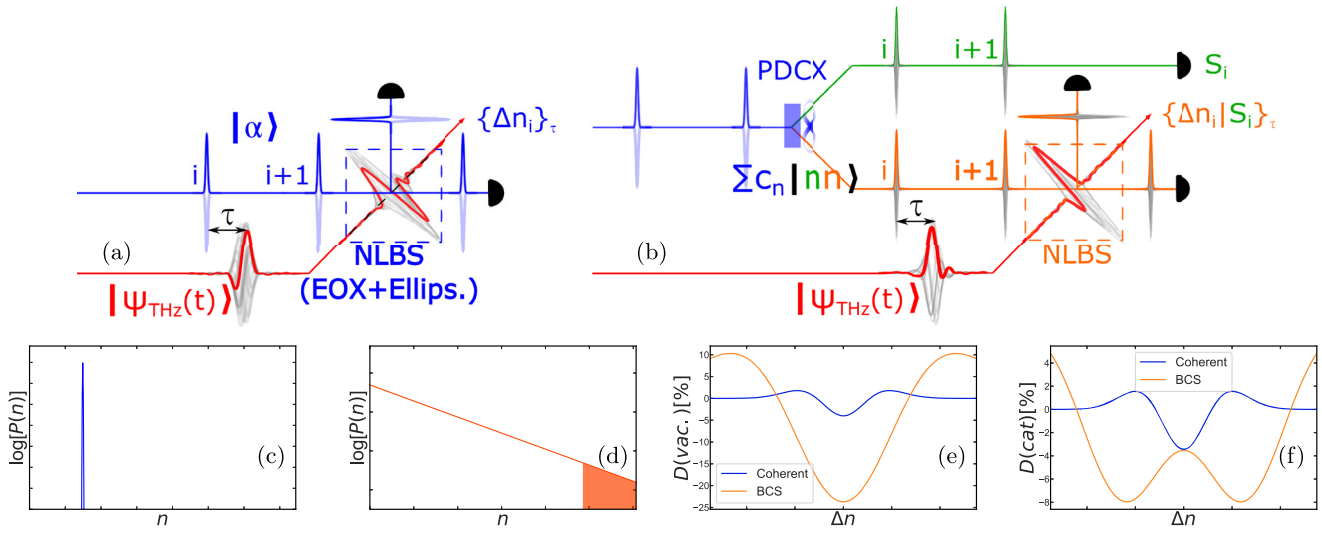

FIG. 1. EOS setups for statistical sampling of quantum states of THz fields. Top row: (a) typical EOS setup, consisting of an EOX, commonly of zinc-blende symmetry (e.g., ZnTe) [17], that mixes an orthogonally polarized ultrashort coherent probe $|\alpha\rangle$ and THz field $|\Psi_{\mathrm{THz}}(t)\rangle$, and an ellipsometry setup (Ellips.) for measuring the weak change in the polarization state of the probe induced by the THz field. These elements are treated as an effective NLBS. The newly proposed scheme (b) replaces the classical probe of (a) by a BCS derived from the parametric down-conversion crystal (PDCX) and conditioned on the intensities measured in a twin branch (in green). Bottom row: (c),(d) logarithms of the probability distributions of the number of photons in the incoming probe (the discreteness is lost in scale) for the coherent state (c) of classical EOS and for (d) a specific BCS, where the orange region is postselected; (e),(f) relative differential noise amplitude D [Eq. (2)] for both cases when the signal is the vacuum state of a confined THz mode such as that of Ref. [4] (e). The amplitude is improved by a little less than 1 order of magnitude. (f) Same comparison for a cat state. There is remarkably little difference between the curves for the coherent probe, while the BCS probe clearly differentiates between vacuum and cat state.

dilation of its space-time volume [4,23]. In this case, the distribution of EOS photocount difference $P(\Delta n;0) = \sum_n P(n)a_0(n,\Delta n)$ depends only on the statistics of the probe, e.g., yielding a Gaussian-distributed shot noise [see Fig. 1(c)] for a classical probe [4]. It is thus judicious to define the relative differential noise amplitude

$$D(\Delta n;\psi) = \frac{P(\Delta n;\psi) - P(\Delta n;0)}{\max[P(\Delta n;0)]}, \tag{2}$$

inspired by Refs. [4,20], where $\max[P]$ is the maximum of the distribution. The magnitude of D gives a quantitative understanding of the contribution of the quantum signal to the overall measurement and acts as a *de facto* signal-to-noise ratio. It is therefore a good optimization target for the EOS scheme.

For an incoming broadband THz vacuum state $|\text{vac.}\rangle$, experiments have shown [4] that mixing in the NLBS results in a $D(\Delta n;\text{vac.})$ signal with a peak-to-peak deviation of about 6%, as shown in Fig. 1(e). It is perhaps not surprising that the weakness of the coupling together with the Gaussian nature of the shot-noise distribution can quickly limit the determination of the full quantum statistics of the signal. As seen from Eq. (1), the photocount distribution in the probe, and hence its second-quantized state, play a significant role in the D measure. Indeed, for classical EOS detection, the best signal-to-noise ratio is achieved when the pulsed probe is devoid of technical noise and thus operates at the shot-noise limit, reached with a coherent state $|\alpha\rangle$ characterized by a Poissonian photocount distribution $P(n)$ centered at $\bar{n} = |\alpha|^2$. Led by this reasoning, one might conclude that the only strategy for improving the value of D is to increase the power of the coherent probe, thus reducing the relative standard deviation in its photocounts. This strategy is already employed in the most optimized experiments so far [4,20,21]. Our proposal demonstrates that it is, in fact, possible to improve the value of D without increasing the average power of the probe.

As we show below, engineering of the second-quantized state of the probe can dramatically enhance the value of D. Perhaps paradoxically, this shows that it can be beneficial to *add* noise to the EOS probe, so long as its correlations are exploited as a resource for metrology [27,39]. In our proposed scheme, this can be accomplished with surprisingly minor modifications of the classical EOS setup. To this end, quantum-enhanced EOS starts with the generation of spatially distinct, single mode in time [40,41] photon-number entangled beams [green and orange lines in Fig. 1(b)] through high-gain nonlinear mixing of a strong classical pump (blue) with the vacuum, in a PDCX [25,27]. One train of the entangled pulses (green) produces photocounts S_i in a square-law detector and the second (orange) is used as a probe in the EOS setup, identical to that of Fig. 1(a). For a given temporal delay τ, the statistical readout of the BPD output Δn_i can now be conditioned on any distribution of the S_i values, yielding various measurement series $\{\Delta n_i|S_i\}_\tau$.

Unconditioned detection of photocounts in either single-mode branch would yield thermal distributions [42–44], with excess noise compared to coherent probes. However, conditioning of one of the measurements on the values of the other now exploits the entanglement properties of the twin beams and can be used to carve desired features in the distribution of photons in the probe. To exemplify this property, Fig. 2 depicts the calculated Wigner quasidistribution of a probe, obtained with the band-conditioned rule $S_i > S_{\text{threshold}}$ [see Fig. 1(d)]. The resulting annular shape of the Wigner representation resembles the conditioning protocol, while also sporting distinct regions of negative values, a hallmark sign of the nonclassicality of the probe's state [42,45].

As displayed in their Wigner representation, BCS probes are quantum in nature and offer distinct advantages that can be used in field-based metrology. To bring this out, we compare side by side the D measures of a coherent and a BCS probe when sampling two distinct cases of incoming quantum fields: a vacuum, and a cat state with a size and coupling to the probe adjusted so that its measured variance is identical to that of the vacuum. In the case of the input vacuum of Ref. [4], the BCS probes (orange line) offer a sixfold increase in amplitude of $D(\Delta n;\text{vac.})$ [Fig. 1(e)]. Even more visible is the advantage of BCSs when applied to the analysis of a few-photon cat state [42,43,45], shown in Fig. 1(f). While the coherent probe (blue line) barely registers any change between $D(\Delta n;\text{vac.})$ and $D(\Delta n;\text{cat})$, the BCS probe shows a remarkable difference between the two quantum signals. To better understand why it is so, we rewrite Eq. (1) as

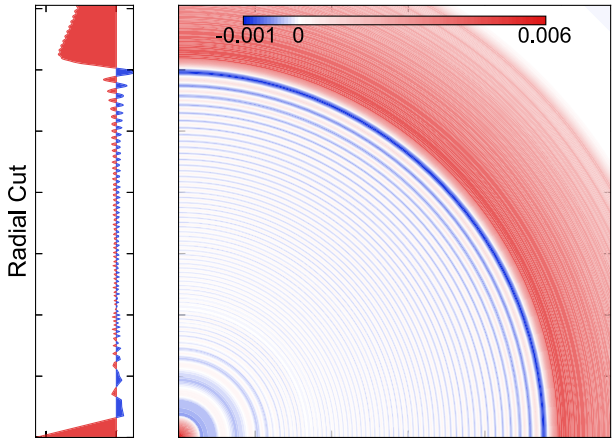

FIG. 2. First quadrant of the rotationally symmetric Wigner quasidistribution of the upper BCS of Figs. 1(d)–1(f). On the left, a radial cut emphasizes the relative size between the positive and negative parts of the distribution. The latter are a direct consequence of the nonclassical nature of this BCS.

$$P(\Delta n;\psi) = \sum_{k=0}^{+\infty} \chi_k(\Delta n)\langle\psi|\hat{\mathcal{E}}^k|\psi\rangle, \tag{3}$$

where $\chi_k(\Delta n)$ represents the susceptibility of the EOS probe to the kth moment of the electric field distribution. Figure 3 compares the susceptibilities of the signal to the first six moments of the electric field distribution for the coherent probe and the BCS probe of Figs. 1(d)–1(f) and 2. Strikingly, the susceptibilities of the coherent probe vanish much quicker with increase in their order, relative to those of the BCS probe. This explains the very different results for the two cases analyzed in Figs. 1(e) and 1(f): a pronounced distinction in the fourth-order moment between the few-photon cat state and the vacuum is clearly discerned by the BCS probe, while remaining almost imperceptible for the coherent case. In fact, the improvement on the measurement of the second moment of the distribution is compounded onto each successive higher moment. This sustained susceptibility to higher-order moments reveals the exciting potential of BCS probes toward robust sampling of strongly nonclassical signals and high-precision quantum state tomography. An additional hallmark of a BCS is its versatility. Conditioning protocols can be engineered to generate very distinct spectra of χ_k functions, as studied in the Supplemental Material for a variety of cases [34]. In particular, it is shown that BCSs conditioned on multiple bands feature noticeable rapidly varying features in their susceptibilities, further aiding in the robust discrimination and full tomography of nontrivial input quantum states.

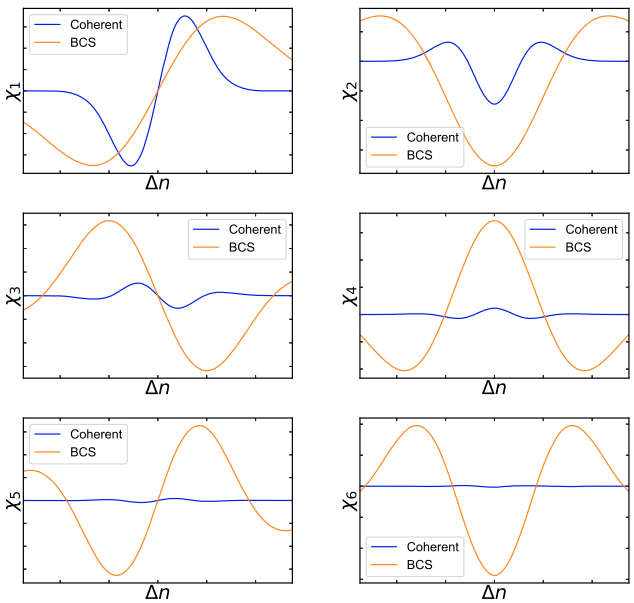

FIG. 3. Susceptibilities to the first six moments of the distribution of the electric field, for a coherent probe (blue lines) and a BCS probe (orange lines). Although the higher moment susceptibilities quickly vanish for the coherent probe, they remain large for the BCS probe, which explains the very different outcomes of Figs. 1(e) and 1(f).

Losses are always detrimental in quantum experiments. As expected for heralded photon sources [46], the metrological advantage of BCSs is sensitive to the imperfections of the setup. To model this, we consider the worst-case scenario arising when all losses occur in a single branch of the PDC output. This scenario leads to the strongest decrease in the correlations between photon numbers in both branches, which is manifested in our model as inability of square-law detectors to act as perfect photon-number resolving devices. By allocating all the "loss budget" to the conditioning branch, we thus determine a strong threshold for total losses in the BCS. Our results [34] show that the advantage of BCSs in EOS vanishes when total losses reach the 50% level. As relatively high quantum efficiency detectors and low-loss optics are readily available across the visible and the near-infrared bands, we believe there is no fundamental technological obstacle to the realization of quantum-enhanced EOS with BCS probes. Furthermore, our scheme could be adapted to loss-tolerant amplification schemes, in line with recent demonstrations of quantum-enhanced metrology with squeezed states [47].

Potential limitation of high-gain PDC schemes can arise from the higher-order nonlinear optical processes, including recently considered pump depletion [48], cascaded nonlinear effects [49], and third-order nonlinearities [50–52]. Practically, these results impose an upper bound on the parametric gain in the PDCX. More work is required to fully understand the implications and possible avoidance strategies of such nonlinear loss mechanisms in quantum applications, but even with those limits, high-gain PDC remains a very efficient mechanism for the production of bright nonclassical states of light.

In conclusion, we introduced electro-optic sampling with band-conditioned states, a class of nonclassical states [27] of light based on bright entangled twin beams derived from spontaneous parametric down-conversion [26], with post-selection on the intensity value of one of the beams. Through a detailed comparison with classical probing, we demonstrated the remarkable promise of these states toward subcycle metrology of quantum fields. Two major improvements on the spectroscopy of quantum fields have been detailed: a sixfold improvement over current experiments, which adds up geometrically for each order of the statistical moments of the field distribution, and versatility in the postselection scheme, which greatly facilitates the process of recovering each successive moment. It thus shatters some of the current limitations of the technique and opens the way to a full tomography of the quantum distribution of THz and mid-IR electric fields. Remarkably, the conditioning protocols can be applied to the raw datasets in postprocessing; it is thus expected that the full power of machine learning algorithms can be applied toward a variety of optimization tasks for robust extraction of

quantum information. In combination with quantum enhancement, the ability to probe the dynamics of quantum fields intrinsically in space-time promises unprecedented experimental access to relativistic quantum electrodynamics and time-domain quantum spectroscopy of matter.

We acknowledge useful discussions with M. Chekhova, A. Moskalenko, N. Quesada, and P. Sharapova. This work was supported by Natural Sciences and Engineering Research Council of Canada (NSERC), via the Canada Research Chair program (CRC), and Fonds de Recherche du Québec –Nature et Technologies (FRQNT), via Institut Transdisciplinaire d'Information Quantique (INTRIQ).

*stephane.virally@polymtl.ca
†denis.seletskiy@polymtl.ca

[1] R. P. Feynman, Space-time approach to quantum electrodynamics, Phys. Rev. **76**, 769 (1949).
[2] M. Collett, R. Loudon, and C. Gardiner, Quantum theory of optical homodyne and heterodyne detection, J. Mod. Opt. **34**, 881 (1987).
[3] A. I. Lvovsky and M. G. Raymer, Continuous-variable optical quantum-state tomography, Rev. Mod. Phys. **81**, 299 (2009).
[4] C. Riek, D. V. Seletskiy, A. S. Moskalenko, J. F. Schmidt, P. Krauspe, S. Eckart, S. Eggert, G. Burkard, and A. Leitenstorfer, Direct sampling of electric-field vacuum fluctuations, Science **350**, 420 (2015).
[5] G. Gallot and D. Grischkowsky, Electro-optic detection of terahertz radiation, J. Opt. Soc. Am. B **16**, 1204 (1999).
[6] T. Brabec and F. Krausz, Intense few-cycle laser fields: Frontiers of nonlinear optics, Rev. Mod. Phys. **72**, 545 (2000).
[7] G. Krauss, S. Lohss, T. Hanke, A. Sell, S. Eggert, R. Huber, and A. Leitenstorfer, Synthesis of a single cycle of light with compact erbium-doped fibre technology, Nat. Photonics **4**, 33 (2010).
[8] M. T. Hassan, T. T. Luu, A. Moulet, O. Raskazovskaya, P. Zhokhov, M. Garg, N. Karpowicz, A. M. Zheltikov, V. Pervak, F. Krausz, and E. Goulielmakis, Optical attosecond pulses and tracking the nonlinear response of bound electrons, Nature (London) **530**, 66 (2016).
[9] J. Valdmanis, G. Mourou, and C. Gabel, Subpicosecond electrical sampling, IEEE J. Quantum Electron. **19**, 664 (1983).
[10] Q. Wu and X. Zhang, Freespace electrooptic sampling of terahertz beams, Appl. Phys. Lett. **67**, 3523 (1995).
[11] A. Leitenstorfer, S. Hunsche, J. Shah, M. C. Nuss, and W. H. Knox, Detectors and sources for ultrabroadband electro-optic sampling: Experiment and theory, Appl. Phys. Lett. **74**, 1516 (1999).
[12] C. Kübler, R. Huber, S. Tübel, and A. Leitenstorfer, Ultrabroadband detection of multi-terahertz field transients with gase electro-optic sensors: Approaching the near infrared, Appl. Phys. Lett. **85**, 3360 (2004).
[13] P. Gaal, M. B. Raschke, K. Reimann, and M. Woerner, Measuring optical frequencies in the 0-40 THz range with non-synchronized electro-optic sampling, Nat. Photonics **1**, 577 (2007).
[14] A. Sell, A. Leitenstorfer, and R. Huber, Phase-locked generation and field-resolved detection of widely tunable terahertz pulses with amplitudes exceeding 100 MV/cm, Opt. Lett. **33**, 2767 (2008).
[15] A. Tomasino, A. Parisi, S. Stivala, P. Livreri, A. C. Cino, A. C. Busacca, M. Peccianti, and R. Morandotti, Wideband THz time domain spectroscopy based on optical rectification and electro-optic sampling, Sci. Rep. **3**, 3116 (2013).
[16] S. Keiber, S. Sederberg, A. Schwarz, M. Trubetskov, V. Pervak, F. Krausz, and N. Karpowicz, Electro-optic sampling of near-infrared waveforms, Nat. Photonics **10**, 159 (2016).
[17] C. Riek, D. V. Seletskiy, and A. Leitenstorfer, Femtosecond measurements of electric fields: From classical amplitudes to quantum fluctuations, Eur. J. Phys. **38**, 024003 (2017).
[18] R. Huber, F. Tauser, A. Brodschelm, M. Bichler, G. Abstreiter, and A. Leitenstorfer, How many-particle interactions develop after ultrafast excitation of an electronhole plasma, Nature (London) **414**, 286 (2001).
[19] P. Jepsen, D. Cooke, and M. Koch, Terahertz spectroscopy and imaging modern techniques and applications, Laser Photonics Rev. **5**, 124 (2011).
[20] C. Riek, P. Sulzer, M. Seeger, A. S. Moskalenko, G. Burkard, D. V. Seletskiy, and A. Leitenstorfer, Subcycle quantum electrodynamics, Nature (London) **541**, 376 (2017).
[21] I.-C. Benea-Chelmus, C. Bonzon, C. Maissen, G. Scalari, M. Beck, and J. Faist, Subcycle measurement of intensity correlations in the terahertz frequency range, Phys. Rev. A **93**, 043812 (2016).
[22] I.-C. Benea-Chelmus, F. F. Settembrini, G. Scalari, and J. Faist, Electric field correlation measurements on the electromagnetic vacuum state, Nature (London) **568**, 202 (2019).
[23] A. S. Moskalenko, C. Riek, D. V. Seletskiy, G. Burkard, and A. Leitenstorfer, Paraxial Theory of Direct Electro-Optic Sampling of the Quantum Vacuum, Phys. Rev. Lett. **115**, 263601 (2015).
[24] F. Lindel, R. Bennett, and S. Y. Buhmann, Theory of polaritonic quantum-vacuum detection, Phys. Rev. A **102**, 041701(R) (2020).
[25] T. S. Iskhakov, A. M. Pérez, K. Y. Spasibko, M. V. Chekhova, and G. Leuchs, Superbunched bright squeezed vacuum state, Opt. Lett. **37**, 1919 (2012).
[26] M. V. Chekhova, G. Leuchs, and M. Zukowski, Bright squeezed vacuum: Entanglement of macroscopic light beams, Opt. Commun. **337**, 27 (2015).
[27] T. S. Iskhakov, V. C. Usenko, U. L. Andersen, R. Filip, M. V. Chekhova, and G. Leuchs, Heralded source of bright multi-mode mesoscopic sub-Poissonian light, Opt. Lett. **41**, 2149 (2016).
[28] S. Virally and B. Reulet, Unidimensional time-domain quantum optics, Phys. Rev. A **100**, 023833 (2019).
[29] M. Kira and S. W. Koch, Quantum-optical spectroscopy of semiconductors, Phys. Rev. A **73**, 013813 (2006).
[30] K. E. Dorfman, F. Schlawin, and S. Mukamel, Nonlinear optical signals and spectroscopy with quantum light, Rev. Mod. Phys. **88**, 045008 (2016).

[31] M. Kira, S. Koch, R. Smith, A. Hunter, and S. Cundiff, Quantum spectroscopy with Schrödinger-cat states, Nat. Phys. **7**, 799 (2011).
[32] S. Mukamel, M. Freyberger, W. Schleich, M. Bellini, A. Zavatta, G. Leuchs, C. Silberhorn, L. L. Boyd, Robert W. Sánchez-Soto, and A. Stefanov, Roadmap on quantum light spectroscopy, J. Phys. B **53**, 072002 (2020).
[33] P. Sulzer, K. Oguchi, J. Huster, M. Kizmann, T. L. M. Guedes, A. Liehl, C. Beckh, A. S. Moskalenko, G. Burkard, D. V. Seletskiy, and A. Leitenstorfer, Determination of the electric field and its hilbert transform in femtosecond electro-optic sampling, Phys. Rev. A **101**, 033821 (2020).
[34] See Supplemental Material at http://link.aps.org/supplemental/10.1103/PhysRevLett.127.270504, which includes Refs. [35–38], for additional details on the theory, and several examples of BCSs.
[35] W. Asavanant, K. Nakashima, Y. Shiozawa, J.-I. Yoshikawa, and A. Furusawa, Generation of highly pure Schrödinger's cat states and real-time quadrature measurements via optical filtering, Opt. Express **25**, 32227 (2017).
[36] A. I. Lvovsky, Squeezed light, arXiv:1401.4118.
[37] C. K. Hong and L. Mandel, Experimental Realization of a Localized One-Photon State, Phys. Rev. Lett. **56**, 58 (1986).
[38] J. Spencer and L. Florescu, *Asymptopia* (American Mathematical Society, New York, 2014).
[39] J. O. Tollerud, G. Sparapassi, A. Montanaro, S. Asban, F. Glerean, F. Giusti, A. Marciniak, G. Kourousias, F. Billè, F. Cilento, S. Mukamel, and D. Fausti, Femtosecond covariance spectroscopy, Proc. Natl. Acad. Sci. U.S.A. **116**, 5383 (2019).
[40] B. Brecht, D. V. Reddy, C. Silberhorn, and M. G. Raymer, Photon Temporal Modes: A Complete Framework for Quantum Information Science, Phys. Rev. X **5**, 041017 (2015).
[41] M. G. Raymer and I. A. Walmsley, Temporal modes in quantum optics: Then and now, Phys. Scr. **95**, 064002 (2020).
[42] M. O. Scully and M. S. Zubairy, *Quantum Optics* (Cambridge University Press, Cambridge, England, 1997).
[43] S. M. Barnett and P. M. Radmore, *Methods in Theoretical Quantum Optics* (Oxford University Press, New York, 1997).
[44] C. W. Gardiner and P. Zoller, *Quantum Noise*, 3rd ed. (Springer, Berlin, Heidelberg, 2004).
[45] H.-A. Bachor and T. C. Ralph, *A Guide to Experiments in Quantum Optics*, 3rd ed. (Wiley, New York, 2019).
[46] S. Virally, S. Lacroix, and N. Godbout, Limits of heralded single-photon sources based on parametric photon-pair generation, Phys. Rev. A **81**, 013808 (2010).
[47] G. Frascella, S. Agne, F. Y. Khalili, and M. V. Chekhova, Overcoming detection loss and noise in squeezing-based optical sensing, npj Quantum Inf. **7**, 72 (2021).
[48] J. Flórez, J. S. Lundeen, and M. V. Chekhova, Pump depletion in parametric down-conversion with low pump energies, Opt. Lett. **45**, 4264 (2020).
[49] A. V. Rasputnyi and D. A. Kopylov, Quantum spatial dynamics of high-gain parametric down-conversion accompanied by cascaded up-conversion, Phys. Rev. A **104**, 013702 (2021).
[50] K. Y. Spasibko, D. A. Kopylov, V. L. Krutyanskiy, T. V. Murzina, G. Leuchs, and M. V. Chekhova, Multiphoton Effects Enhanced Due to Ultrafast Photon-Number Fluctuations, Phys. Rev. Lett. **119**, 223603 (2017).
[51] N. Quesada, G. Triginer, M. D. Vidrighin, and J. E. Sipe, Theory of high-gain twin-beam generation in waveguides: From Maxwell's equations to efficient simulation, Phys. Rev. A **102**, 033519 (2020).
[52] G. Triginer, M. D. Vidrighin, N. Quesada, A. Eckstein, M. Moore, W. S. Kolthammer, J. E. Sipe, and I. A. Walmsley, Understanding High-Gain Twin-Beam Sources Using Cascaded Stimulated Emission, Phys. Rev. X **10**, 031063 (2020).